We are IntechOpen, the world's leading publisher of Open Access books Built by scientists, for scientists

4,800
Open access books available

122,000
International authors and editors

135M
Downloads

Our authors are among the

154
Countries delivered to

TOP 1%
most cited scientists

12.2%
Contributors from top 500 universities

CLARIVATE ANALYTICS BOOK CITATION INDEX INDEXED

WEB OF SCIENCE™

Selection of our books indexed in the Book Citation Index in Web of Science™ Core Collection (BKCI)

Interested in publishing with us?
Contact book.department@intechopen.com

Numbers displayed above are based on latest data collected.
For more information visit www.intechopen.com

22

$BiFeO_3$ Thin Films Prepared by Chemical Solution Deposition with Approaches for Improvement of Ferroelectricity

Yoshitaka Nakamura, Seiji Nakashima and Masanori Okuyama
Graduate School of Engineering Science, Osaka University
Japan

1. Introduction

Bismuth ferrite ($BiFeO_3$) is one of the most promising lead-free ferroelectric materials. Both bulk and thin film forms have been investigated and found a remarkably large ferroelectric polarization as well as *G*-type antiferromagnetism, often called it as multiferroics having ferroelectricity, magnetism, and ferroelasticity. There are several thin film fabrication methods including pulsed laser deposition, metal organic chemical vapour deposition, sputtering, and chemical solution deposition for this material. In this chapter, we describe the basic property of $BiFeO_3$ and the general outline of chemical solution deposition.

1.1 Crystal structure of $BiFeO_3$

Bulk $BiFeO_3$ shows a rhombohedral symmetry (point group *R*3c) with lattice parameters of a = 0.396 nm and α = 89.6° at room temperature (RT). Its transition temperature was investigated by Roginskaya et al. and a structural change showed at around 1100 K (Roginskaya et al., 1963). A detailed crystalline structure above the transition temperature has been investigated by Palai et al.. They reported that the transition temperature from rhombohedral to orthorhombic symmetry was at around 1100 K as well as orthorhombic to cubic symmetry at around 1200 K (Palai et al., 2008).

1.2 Electrical property of $BiFeO_3$

Rhombohedral $BiFeO_3$ has a ferroelectric polarization along [111]. Polarization of the single crystal was measured and showed small polarizations of 6.1 μC/cm² along [111] and 3.5 μC/cm² along [100] at 80 K (Teague et al., 1970). These small polarizations are regarded as low sample-quality now. Recent reports showed saturated polarizations of ~60 μC/cm² with single crystals as well as ~40 μC/cm² with ceramics measured at RT (Lebeugle et al., 2007; Shvartsman et al., 2007).

Recent study has also been focused on $BiFeO_3$ thin films. A saturated polarization of 55 μC/cm² along [001] was reported from epitaxial films on $SrRuO_3/SrTiO_3$ (001) substrates measured at RT (Wang et al., 2003; Li et al., 2004). Films also showed ferroelectric polarizations of 80 μC/cm² on $SrTiO_3$ (110) and 100 μC/cm² on $SrTiO_3$ (111), having an equivalent relationship between $\sqrt{3}P_{(001)}$, $\sqrt{2}P_{(101)}$, and $P_{(111)}$ (Li et al., 2004). Moreover, a giant ferroelectric polarization beyond 150 μC/cm² has been reported from polycrystalline $BiFeO_3$

thin films with a tetragonal structure measured at 80 K (Yun et al., 2004). Recent theoretical calculation showed a polarization of about 100 μC/cm² in a rhombohedral structure as well as about 150 μC/cm² in a tetragonal structure. These values showed a good agreement with the experimental ones (Ederer et al., 2006; Ricinschi et al., 2006).

1.3 General outline of chemical solution deposition

Chemical solution deposition (CSD) is one of the thin film fabrication methods, and it includes spin-coating, drying and annealing processes. Precursor solution is deposited onto a substrate by a spin-coating process. After the spin-coating process, a film dying process is carried out to evaporate the solvent and decompose metal-organic compounds in the precursor. An amorphous film is obtained at this stage. These processes are repeated several times to obtain a desired film thickness. For the film crystallization, an annealing process is carried out. It is usually carried out by a rapid thermal annealing (RTA) equipment to crystallize and densify the film. Higher heating rate usually decomposes metal organic compounds quickly and then desired oxide films with a higher density can be obtained (Schwartz, 1997).

There are some advantages for CSD; (i) uniformity of the molecules in precursor solutions and thin films, (ii) control of the film thickness by changing the solution concentration or the coating speed, (iii) control of the composition ratio by mixing solutions, (iv) film fabrication in ambient pressure, (v) synthesis of a non-equilibrium phase by the low-temperature process. However, there are some disadvantages for this method; (i) possibility of cracks in a film fabrication process, (ii) contamination which results in a difficulty of the manufacturing process, (iii) films with low-coherency comparing with other thin film fabrication methods such as pulsed laser deposition, chemical vapor deposition, and molecular beam epitaxy.

1.4 Precursor solutions for $BiFeO_3$

Precursor solutions for the CSD method are distinctly important. They consist of metal organic compounds and solvent which determine process parameters such as drying and annealing temperatures, film thickness per one spin-coating process, and coating affinity to the substrates. In this chapter, $BiFeO_3$ thin films were prepared by CSD with precursor solutions using 2-ethylhexanoate bismuth $[Bi(OCO(CH)(C_2H_5)C_4H_9)_3]$ and trisacetylacetonato iron $[Fe(C_5H_7O_2)_3]$ as metal organic materials, and toluene as a solvent.

2. Ferroelectric property of $BiFeO_3$ thin films prepared by CSD with controlling Bi/Fe ratio in the precursor solution

In this section, we demonstrate the $BiFeO_3$ thin film growth with controlling Bi/Fe ratio of the precursor solutions. Composition ratio affects the crystal growth and the electric property of the films. We obtain both good crystallinity and ferroelectric polarization of 85 μC/cm² with films using 10 mol% Bi-excess solution (Nakamura et al., 2007; Nakamura et al., 2008).

2.1 Film preparation by CSD with controlling Bi/Fe ratio

$BiFeO_3$ thin films were deposited on a Pt (200 nm)/TiO_2 (40 nm)/SiO_2 (600 nm)/Si substrate by CSD using precursor solutions of different Bi/Fe ratios: 10 mol% Fe-excess (10%Fe-ex.), stoichiometric, 5 mol% Bi-excess (5%Bi-ex.), 10 mol% Bi-excess (10%Bi-ex.), and 20 mol% Bi-

excess (20%Bi-ex.). The precursor solution was spin-coated at 3000 rpm for 30 s and dried at 250°C for 5 min in air. These processes were repeated 20 times to obtain a film thickness of 250 nm. Then the films were annealed at 450 °C for 15 min in nitrogen atmosphere using the RTA equipment. For electrical measurement, Pt top electrodes with a diameter of 190 μm and a thickness of 100 nm were formed on the films by rf sputtering at RT. We confirmed by inductively coupled plasma (ICP) analysis that the composition ratios of $BiFeO_3$ thin films were the same as the precursor solutions.

2.2 Crystal structure

Figure 1 shows θ–2θ scans of the XRD patterns of the $BiFeO_3$ thin films with different Bi/Fe ratios. All the films show polycrystalline perovskite phase mainly. However, the 10%Fe-ex. $BiFeO_3$ film has small amount of a $Bi_2Fe_4O_9$ phase and the 20%Bi-ex. film shows a Bi_2O_3 phase. This indicates that excessive Fe or Bi compounds in the precursor solution tend to form impurity phase. Comparing the peak intensities corresponding to the (010) and (110) planes, the 10%Bi-ex. and 20%Bi-ex. films show higher diffraction intensities, indicating that they are crystallized well. This result suggests that Bi compounds in the precursor solution contribute the promotion of the film crystallization but that 5 mol% excess Bi is insufficient for the crystallization of such films.

2.3 Surface texture and raman spectrum

Figures 2(a-e) show the atomic force microscope (AFM) images of $BiFeO_3$ films taken in a 20 × 20 μm² area. All the $BiFeO_3$ thin films show a rosette structure, which consists of circular regions with an uneven texture and outer regions with a flat surface. These structures were also reported in $PbZrO_3$ thin films prepared by the sol–gel method (Alkoy et al., 2005). Table I shows the percentages of circular regions, RMS roughnesses and total boundary lengths surrounding the circular regions evaluated from Figs. 2(a-e). As can be seen in Table I, the percentage of circular region and RMS roughness tend to increase with an increase in Bi/Fe ratio. On the other hand, the total boundary length is ~200 μm and seems to have no systematic dependence.

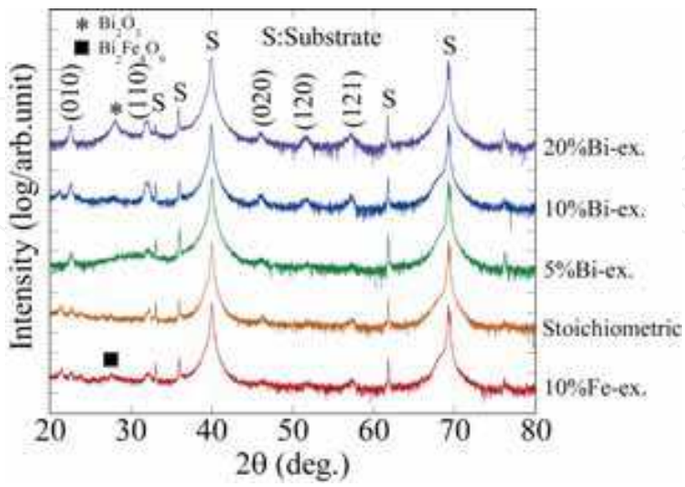

Fig. 1. XRD θ–2θ patterns of $BiFeO_3$ thin films prepared using 10 mol%Fe-excess (10%Fe-ex.), stoichiometric, 5 mol% Bi-excess (5%Bi-ex.), 10 mol% Bi-excess (10%Bi-ex.), and 20 mol% Bi-excess (20%Bi-ex.) precursor solutions.

Figure 3(a) shows an AFM image of the 10%Bi-ex. $BiFeO_3$ thin film with white circles marking the measurement location of Raman spectroscopy. A laser with a 0.7 μm spot size and an excitation wavelength of 515 nm was applied to the film surface labelled "Circular region" and "Outer region" in Fig. 3(a). Figure 3(b) shows the Raman spectra measured at RT in each measurement location shown in Fig. 3(a). The spectrum measured in $BiFeO_3$ ceramic is also shown as a reference. As shown in Fig. 3(b), the spectrum measured in the circular region is almost similar to that of $BiFeO_3$ ceramic consisting of polycrystalline grains. On the other hand, the spectrum measured in the outer region has a broad shape, found frequently in amorphous materials, and is different from that of $BiFeO_3$ ceramic.

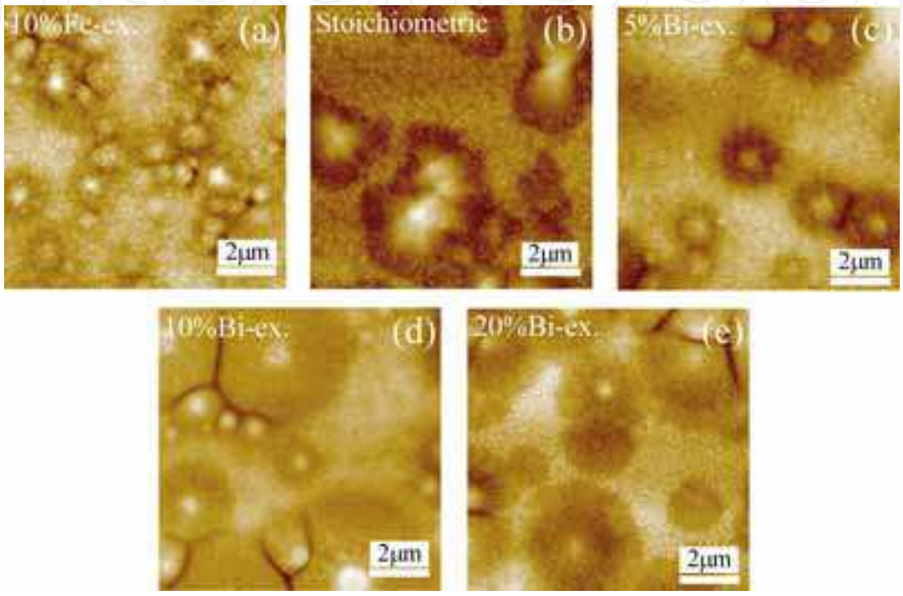

Fig. 2. 20 × 20 μm² surface AFM images for the $BiFeO_3$ films of (a) 10%Fe-ex., (b) stoichiometric, (c) 5%Bi-ex., (d) 10%Bi-ex., and (e) 20%Bi-ex.. Each film shows a rosette structure, which consists of circular regions and outer regions.

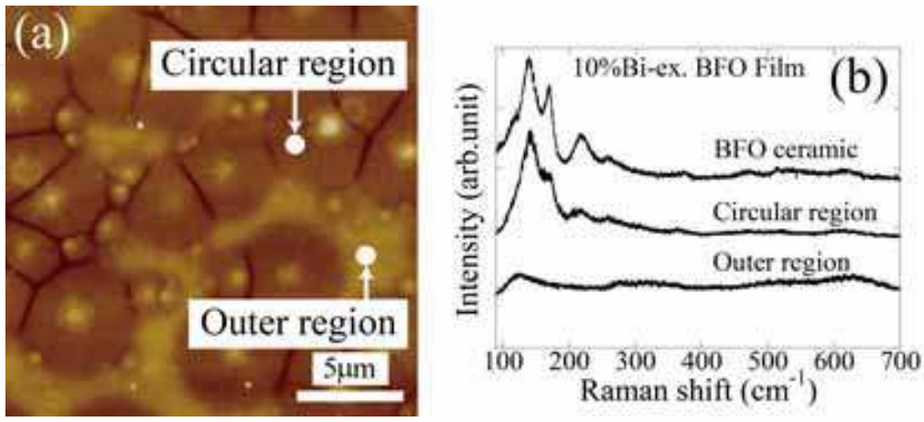

Fig. 3. (a) AFM image of 10%Bi-ex. $BiFeO_3$ thin film with white circle marking the measurement location of Raman spectroscopy. (b) Raman spectra measured at RT for each location shown in (a). Spectrum of $BiFeO_3$ ceramic is also shown as a reference.

Sample	Circular region area (%)	RMS roughness (nm)	Boundary length (mm)
10%Fe-ex.	46.0	3.6	238
Stoichiometric	48.1	5.1	225
5%Bi-ex.	41.1	5.6	196
10%Bi-ex.	85.9	4.8	165
20%Bi-ex.	53.7	6.8	208

Table 1. Circular region areas, RMS roughnesses, and boundary lengths for all samples.

The same results are also obtained in $BiFeO_3$ thin films prepared using the other precursor solutions with different Bi/Fe ratios. These results indicate that the circular regions have a $BiFeO_3$ crystalline phase, while the outer regions have an amorphous $BiFeO_3$ phase. Moreover, it can be considered that each phase exists from the top to the bottom of the film in a vertical direction because the excitation can sufficiently penetrate up to the bottom of the film. Consequently, the $BiFeO_3$ thin films of 10%Bi-ex. and 20%Bi-ex. have more circular regions and show good crystallinity, as shown in Fig. 1. This tendency is also observed in the $Pb(Zr,Ti)O_3$ (PZT) thin film prepared by the sol–gel method. Excessive Pb compounds in the precursor solution promote the formation of PZT and lead to show more circular regions (Alkoy et al., 2005). From Figs. 1 and 2, however, the 20%Bi-ex. film shows a Bi_2O_3 phase, and the area of circular regions does not seem to increase so much compared with that in the 10%Bi-ex. film. This result suggests that excessive Bi compounds in the precursor solution are more reactive, thereby they promote the formation of $BiFeO_3$. However, the major amount of Bi compounds tends to form Bi_2O_3 as well as $BiFeO_3$, therefore the circular region does not seem to increase so much.

2.4 Ferroelectric property

Figure 4(a) shows the leakage current density versus electric field (*J*–*E*) property of the $BiFeO_3$ thin films measured at RT. A comparatively larger leakage current is obtained in the films that contain more Bi. Figure 4(b) shows *P*–*E* hysteresis loops of the $BiFeO_3$ thin film measured at RT with a scanning frequency of 20 kHz. The 10%Bi-ex. $BiFeO_3$ thin film shows more squareness in hysteresis loop than the other films. The remanent polarizations (P_r) for the maximum applied electric field of 1.2 MV/cm are 30, 38, 28, 85, and 53 μC/cm² for the films of 10%Fe-ex., stoichiometric, 5%Bi-ex., 10%Bi-ex., and 20% Bi-ex., respectively.

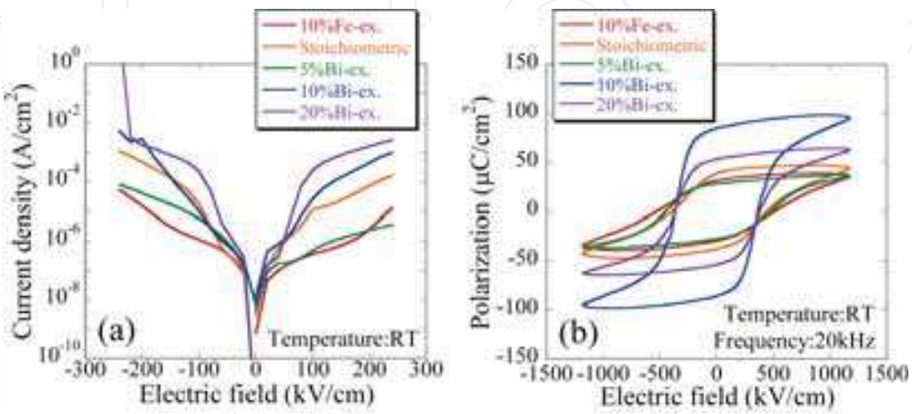

Fig. 4. (a) *J*–*E* characteristics of $BiFeO_3$ thin films measured at RT. (b) *P*–*E* hysteresis loops measured at RT.

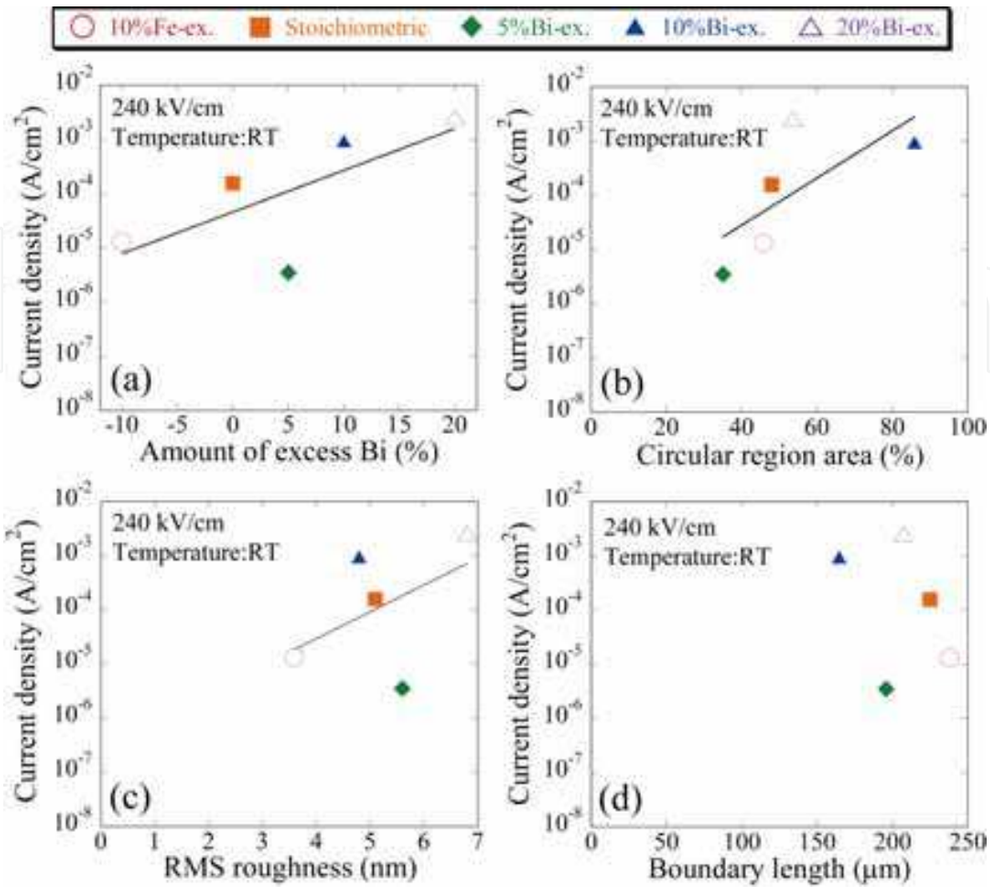

Fig. 5. Leakage current of $BiFeO_3$ thin films at 240 kV/cm as function of (a) amount of excess Bi, (b) percentage of circular region area, (c) RMS roughness, and (d) boundary length.

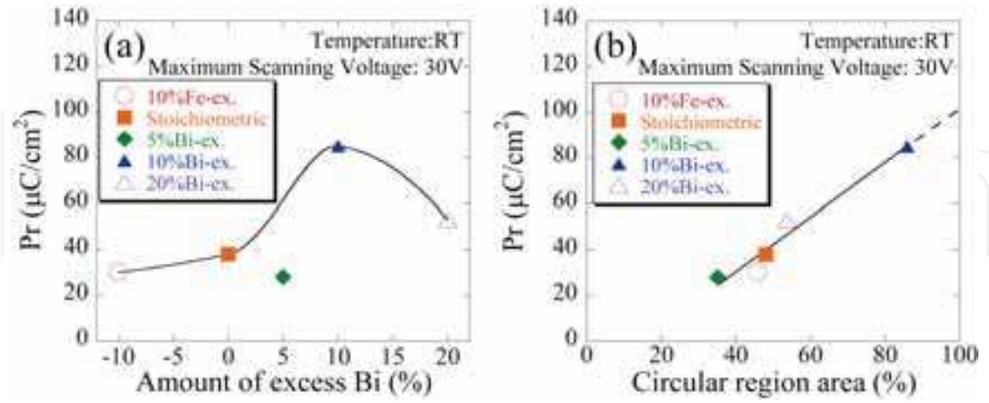

Fig. 6. Remanent polarization of $BiFeO_3$ thin films as function of (a) amount of excess Bi and (b) percentage of circular region area.

2.5 Relationship between surface texture and ferroelectricity

To investigate the influences of the surface texture and Bi/Fe ratio on the leakage current of $BiFeO_3$ thin films, we consider the amount of excess Bi, percentage of circular region area,

RMS roughness, and boundary length at the surface between crystal and amorphous phases, as shown in Table I. Figures 5(a-d) show the leakage current measured at 240 kV/cm versus (a) amount of excess Bi, (b) circular region area, (c) RMS roughness, and (d) boundary length. As shown in Figs. 5(a-c), leakage current tends to exponentially increase with an increase in the amount of excess Bi, circular region area, and RMS roughness although some scattering of the data is observed in Fig. 5(c). On the other hand, the length between the circular regions and the outer regions does not seem to affect the leakage current as shown in Fig. 5(d). These results suggest that the $BiFeO_3$ thin film prepared using the Bi excess precursor solution tends to have more circular regions that have $BiFeO_3$ crystals and to have a larger RMS roughness. From these leakage trends, leakage current mainly passes through circular regions consisting of crystalline $BiFeO_3$ rather than through outer amorphous region, and that current is increased by a rough surface. We further investigate the influences of the surface texture and Bi/Fe ratio on the ferroelectric polarization of $BiFeO_3$ thin films. We plot the amount of excess Bi and percentage of circular region area that has $BiFeO_3$ crystals, as shown in Fig. 3(b). Figures 6(a) and 6(b) show the remanent polarization measured at RT versus (a) amount of excess Bi and (b) circular region area. The remanent polarization increases with an increase in Bi ratio below the 10%Bi-ex. $BiFeO_3$ film. However, the 20%Bi-ex. film decreases its remanent polarization because of the mixed phase of $BiFeO_3$ and Bi_2O_3. As shown in Fig. 6(b), the remanent polarization linearly increases with an increase in the percentage of the circular region area. From the extrapolated line in Fig. 6(b), fully crystallized $BiFeO_3$ thin films are expected to show 100 $\mu C/cm^2$. According to leakage and polarization plots in Fig. 5 and Fig. 6, a 10 mol% Bi-excess solution gives $BiFeO_3$ thin films the best ferroelectric property with more circular regions.

3. Insertion effect of Bi-excess layer on $BiFeO_3$ thin films

In section 2, Bi-excess solution, or precursor solution with excessive Bi compounds, promotes film crystallization, leading to a good ferroelectricity. In this section, we demonstrate the insertion effect of Bi-excess layer to the stoichiometric $BiFeO_3$ thin films to improve the crystal growth and ferroelectricity of the films (Nakamura et al., 2007; Nakamura et al., 2008).

3.1 Insertion effect

Insertion effect, inserting Bi-excess $BiFeO_3$ layer to the film, is aiming to promote the crystal growth of the film and to obtain a good ferroelectricity. There are some reports that ferroelectric thin films prepared by CSD show a non-crystalline layer at the interface between the thin film and the electrode. Such a layer is reported as an interfacial layer which degrades the ferroelectric property of the film (Grossmann et al., 2002). These reports suggest that the low crystallinity part is concentrated at the interface between the film and the electrode. To improve the low crystallinity part, an insertion layer promoting crystal growth will be effective.

In our $BiFeO_3$ thin films, a thin film with stoichiometric solution shows low crystallinity with a small polarization, and a film with 10 mol% Bi-excess solution shows high crystallinity and a large polarization. Thus an insertion layer with 10 mol% Bi-excess solution is expected to be effective. To investigate the insertion effect of Bi-excess layers, three types of thin films were prepared on $Pt/TiO_2/SiO_2/Si$ substrates, as shown in Fig. 7: stoichiometric $BiFeO_3$ thin film with Bi-excess top layer (Bi-T), bottom layer (Bi-B), and top

and bottom layer (Bi-TB). Then the films were annealed at 450 °C for 15 min in a nitrogen atmosphere using the RTA process. For the electrical measurement, Pt top electrodes with a diameter of 190 μm were formed by rf sputtering.

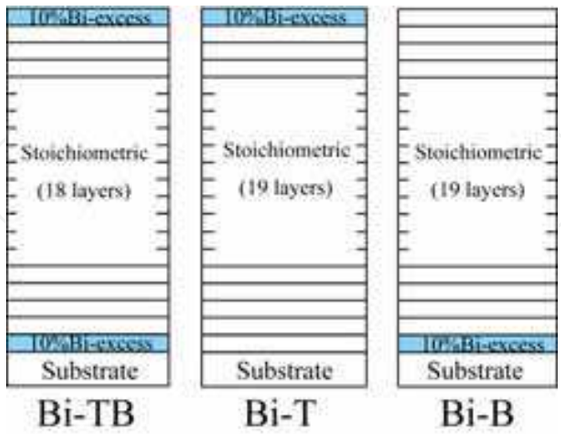

Fig. 7. Schematic models of $BiFeO_3$ thin films inserting Bi-excess top and bottom layer (Bi-TB), top layer (Bi-T), and bottom layer (Bi-B).

3.2 Crystal structure

Figure 8 shows the θ–2θ scans of XRD patterns of the $BiFeO_3$ thin films with Bi-excess top and bottom layer (Bi-TB), top layer (Bi-T), and bottom layer (Bi-B). These results show that all the films exhibit mainly polycrystalline perovskite single phase without nonperovskite phases such as $Bi_2Fe_4O_9$ and Bi_2O_3. Comparing peak intensities corresponding to (010) and (110) planes, the crystallinity of Bi-TB is the best. Bi-T is the second best, followed by Bi-B. This result indicates that the Bi-excess top layer improves the crystallization in the annealing process. Moreover, this tendency suggests that the crystallization is produced from the surface to the bottom using the RTA process. As for the difference between Bi-TB and Bi-T, crystallinity of $BiFeO_3$ film can be enhanced by inserting the Bi-excess layer on the top surface and the bottom.

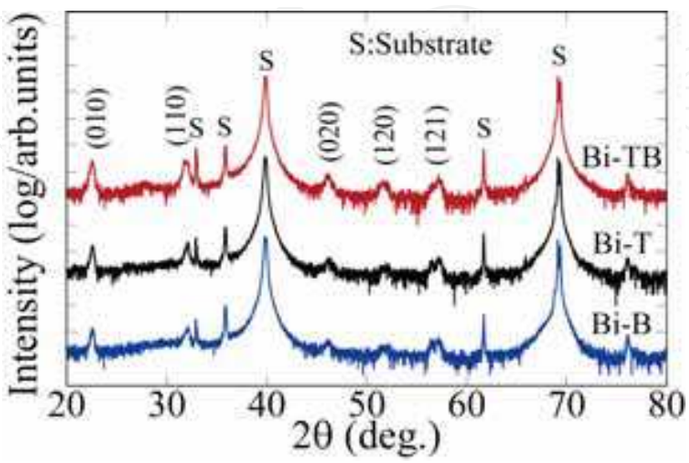

Fig. 8. XRD θ–2θ patterns of Bi-TB, Bi-T, and Bi-B $BiFeO_3$ thin films.

3.3 Surface texture and raman spectrum

Figures 9(a-c) show the AFM images of $BiFeO_3$ films taken over a 10 × 10 μm² area. As can be seen in Fig. 9(a), Bi-TB forms more grains than the others. On the other hand, Bi-T and Bi-B form finer grains as well as larger grains, as shown in Figs. 9(b) and 9(c). In addition, Bi-T seems to form larger grains than the film of Bi-B. The surface RMS roughness is estimated as 7.7, 6.7, and 5.0 nm for the films of Bi-TB, Bi-T, and Bi-B, respectively. The number of grains and the surface roughness increase with increasing crystallinity, comparing Fig. 9 with Fig. 8. To investigate the difference between finer and larger grains, Raman spectroscopy was carried out. A laser with a 0.7 μm spot size irradiated the points labelled A–C, which form large grains, and D–F, which form fine grains, as shown in Figs. 9(a-c). Figures 9(d) and 9(e) show Raman spectra measured at RT. These figures also include the spectrum measured in $BiFeO_3$ ceramic, as a reference. As shown in Fig. 9(d), the spectra measured in the areas A–C are almost the same as the spectrum of $BiFeO_3$ ceramic. On the other hand, the spectra measured in the areas D–F are different from the spectrum of $BiFeO_3$ ceramic, as shown in Fig. 9(e). These results indicate that the areas A–C have good $BiFeO_3$ crystals while the areas D–F seem to be amorphized. Moreover, the area at which the $BiFeO_3$ crystal spectrum was observed is the largest in Bi-TB. This result relates that Bi-TB crystallizes the best, comparing Figs. 9 and 8.

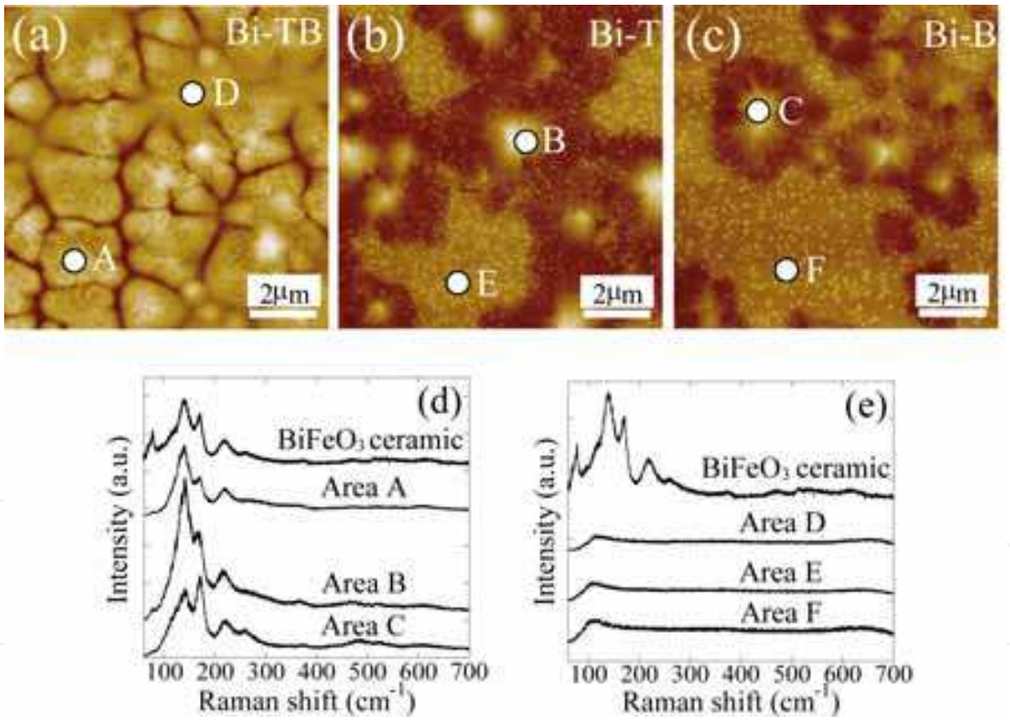

Fig. 9. 10 × 10 μm² surface AFM images with markings of the typical locations of Raman spectroscopy for the films of (a) Bi-TB, (b) Bi-T, and (c) Bi-B, respectively. Areas A–C form large grains, while areas D–F form fine grains. (d) and (e) Raman spectra measured at RT for the locations shown in Figs. 9(a)–9(c).

3.4 Ferroelectric property

Figure 10 shows the leakage current density versus electric field (*J*–*E*) of $BiFeO_3$ thin films measured at (a) RT and (b) 80 K. When the electric field is lower than 300 kV/cm, the

leakage currents are almost unchanged among three types of films both at RT and 80 K. This suggests that the amorphous phase of the surface limits the conduction in the case of lower electric field, as mentioned in Abe et al. (Abe et al., 1993). On the other hand, when the electric field is higher than 300 kV/cm at 80 K, the leakage current becomes large for the film of Bi-TB. Therefore, it is suggested that the amorphous phase includes defects that limit the carrier emission at the interface, and the leakage current increases at higher electric fields in the Bi-TB film. In the case of Bi-T and Bi-B, the amorphous phase might suppress the leakage current at high electric field. Figure 11 shows ferroelectric polarization versus electric field (*P*–*E*) hysteresis loops of $BiFeO_3$ thin film at (a) RT and (b) 80 K, respectively. At RT, the remanent polarizations (P_r) for maximum applied electric field of 1.0 MV/cm are 55, 26, and 17 μC/cm² for the films of Bi-TB, Bi-T, and Bi-B, respectively. In addition, the coercive field of Bi-TB is 385 kV/cm, which is the lowest in the three types of films. At 80 K, the remanent polarizations for maximum applied electric field of 2.0 MV/cm are 65, 46, and 32 μC/cm² for the films of Bi-TB, Bi-T, and Bi-B, respectively. The remanent polarization of Bi-TB is about twice that of the film prepared by stoichiometric solution (28 μC/cm² at RT, and 38 μC/cm² at 80 K). These results show that $BiFeO_3$ thin film of Bi-TB gives the best ferroelectric property among the three types of films, which is attributed to the good crystallinity of the $BiFeO_3$ film, comparing Figs. 11 and 8.

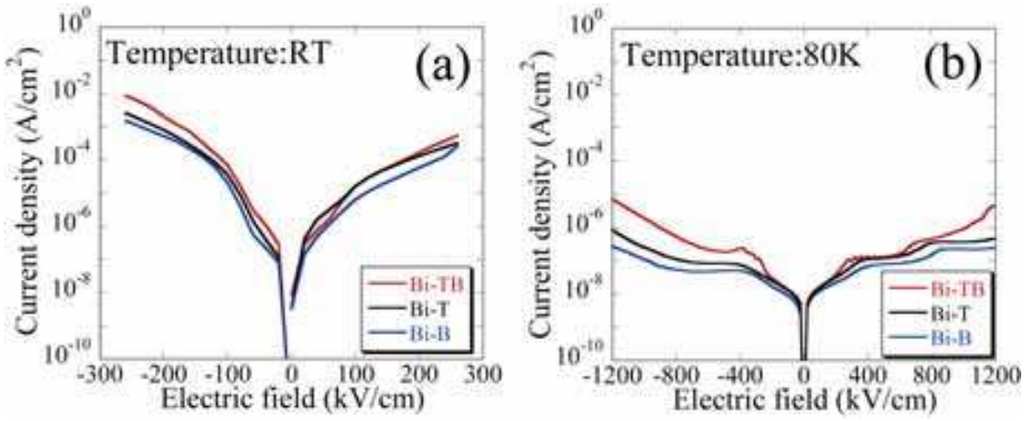

Fig. 10. Leakage current characteristics of $BiFeO_3$ thin films measured at (a) RT and (b) 80 K.

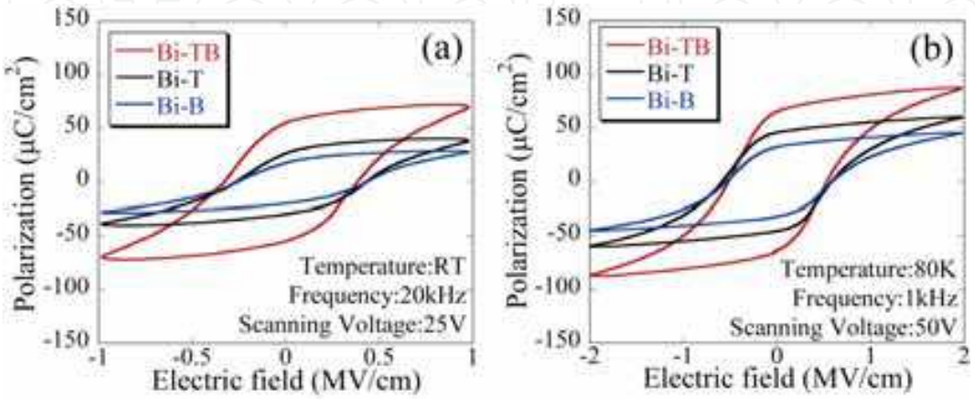

Fig. 11. *P*–*E* hysteresis loops of $BiFeO_3$ thin films measured at (a) RT and (b) 80 K.

4. Improvement of ferroelectricity of $BiFeO_3$ thin films by postmetallization annealing and electric field application

In this section, we describe the postmetallization annealing and electric field application by using 10 mol% Bi-excess $BiFeO_3$ thin film which shows good ferroelectricity in section 2. These are the ways to improve ferroelectricity of $BiFeO_3$ thin films. Postmetallizaton annealing is the electrode annealing process to reduce the leakage current which has already reported in several thin film materials such as $BaTiO_3$, $(Ba,Sr)TiO_3$, $(Pb,Sr)TiO_3$, and PZT after the deposition of top electrodes (Lee et al., 2004; Joo et al., 1997; Chung et al., 2001; Thakoor, 1994). Electric field application is to apply a high electric field to reverse its polarization reversal easily. It is typically carried out in bulk materials such as PZT (Kamel et al., 2007). These two approaches are expected to be effective to improve ferroelectric properties of $BiFeO_3$ thin films (Nakamura et al., 2009).

4.1 Film preparation methods

$BiFeO_3$ thin films were deposited on a $Pt/TiO_2/SiO_2/Si$ substrate by CSD using 10mol % Bi-excess precursor solution. Spin-coating and drying processes were the same as in chapter 2. These processes were repeated 20 times to obtain a film thickness of 250 nm. Then, the films were treated by the RTA process at 450 °C for 20 min in nitrogen atmosphere. For the electrical measurement, Pt top electrodes were formed on the $BiFeO_3$ film by rf sputtering. After the deposition of Pt top electrodes, the sample was divided into three pieces and labelled as BFO, BFO-N, and BFO-O, respectively. Then the postmetallization annealing was carried out for 5 min at 300 °C in nitrogen atmosphere for BFO-N, and oxygen atmosphere for BFO-O by the RTA process. Finally, the following three films were obtained; BFO (as prepared film without postmetallization annealing), BFO-N (the film with the annealing in nitrogen atmosphere), and BFO-O (the film with the annealing in oxygen atmosphere).

4.2 Improvement of ferroelectric property of $BiFeO_3$ thin films by postmetallization annealing

Figure 12(a) shows the θ-2θ patterns of the XRD of the $BiFeO_3$ thin films with and without the postmetallization annealing. All the films consist mainly of polycrystalline perovskite phase, but a Bi_2O_3 phase is slightly observed. Evaluating the diffraction peak intensity of each film, it does not change among three films. This result indicates that the crystallinity of $BiFeO_3$ does not change by the postmetallization annealing. We note that the intensity of an observed Bi_2O_3 phase is much smaller than the $BiFeO_3$ phase and its intensity does not change after the postmetallization annealing. Therefore, it is enough to evaluate the dielectric property of $BiFeO_3$ and the annealing effect of the electrode. There may be a possibility of a peak shift due to a strain relaxation between the $BiFeO_3$ film and the Pt electrode by the postmetallization annealing, however, it is hard to observe the strain relaxation from such a small 190 μm diameter dot electrode because an incident X-ray beam width is about 2 mm, making it difficult to analyze the crystalline property of the small area. To confirm the strain relaxation, a 100 nm thick Pt film was deposited on the whole $BiFeO_3$ film surface and then the postmetallization annealing was carried out. Figure 12(b) shows the XRD patterns near (010) peak before and after the Pt deposition and the postmetallization annealing in nitrogen atmosphere. The peak intensity is decreased due to the deposition of the Pt film, but the peak shift is not observed. This result suggests that a clear strain relaxation does not occur near the interface between the $BiFeO_3$ film and the Pt electrode after the postmetallization annealing.

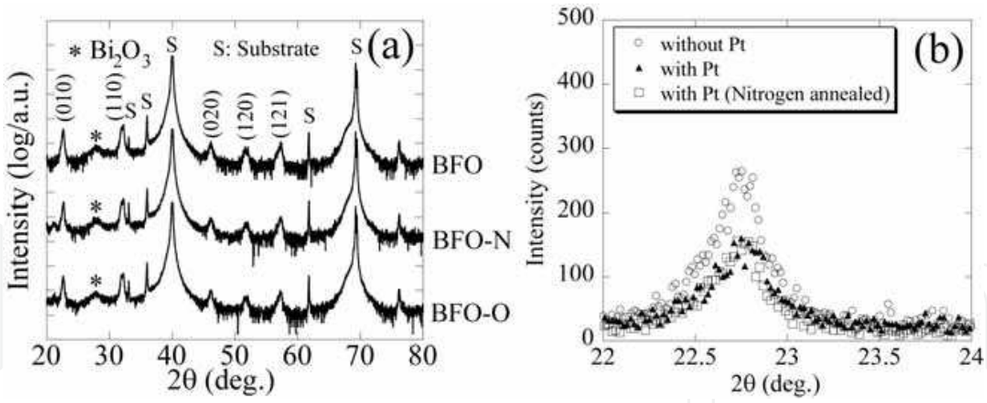

Fig. 12. (a) XRD θ-2θ scans of as-prepared (BFO), N_2 annealed (BFO-N), and O_2 annealed (BFO-O) $BiFeO_3$ thin films. (b) Expanded scans near the (010) peak before and after the Pt deposition and the postmetallization annealing. A 100 nm thick of Pt film was deposited on the whole surface of the $BiFeO_3$ film.

Figures 13(a) and 13(b) show the *J-E* characteristics of $BiFeO_3$ thin films measured at (a) 80 K and at (b) RT. The leakage current is suppressed in both the BFO-N and BFO-O films at 80 K. This suppression is also observed at RT. Joo et al. reported that the leakage current is suppressed by the postmetallization annealing in oxygen atmosphere due to the reduction of oxygen vacancies in a film (Joo et al., 1997). Contrary to their result, our result suggests that the postmetallization annealing improves the contact between the $BiFeO_3$ film and the Pt electrode or the reduction of defects near the interface between the $BiFeO_3$ film and the Pt electrode as suggested in Pt/PZT/Pt capacitors, rather than the compensation of oxygen vacancies in the $BiFeO_3$ film.

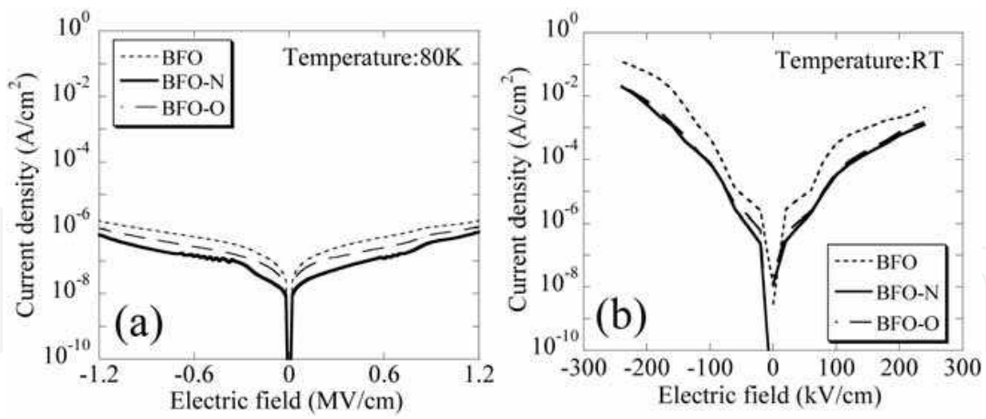

Fig. 13. Current density-electric field (*J-E*) characteristics of $BiFeO_3$ thin films measured at (a) 80 K and at (b) RT.

Figures 14(a) and 14(b) show frequency dependences of the dielectric constant and the dielectric loss tan δ measured at (a) 80 K and at (b) RT. The dielectric constant and the loss tangent of $BiFeO_3$ thin films measured at 80 K are found to be 185 and 0.061, 172 and 0.045, and 186 and 0.048 for the BFO, BFO-N, and BFO-O film with a measuring frequency of 1 MHz, respectively. In addition, the frequency variability of from 10^3 to 10^6 Hz is 20.5% BFO, 16.9% BFO-N, and 18.3% BFO-O. The reduction in the frequency variability and the

dielectric loss may be due to the reduction in the leakage current as shown in Fig. 13(a). The same tendencies are also observed in the $BiFeO_3$ films measured at RT, as shown in Fig. 13(b). The frequency variability from 10^3 to 10^6 Hz is 30.6% BFO, 23.3% BFO-N, and 23.4% BFO-O measured at RT. These results indicate that the frequency variability of and the dielectric loss are successfully reduced by the postmetallization annealing.

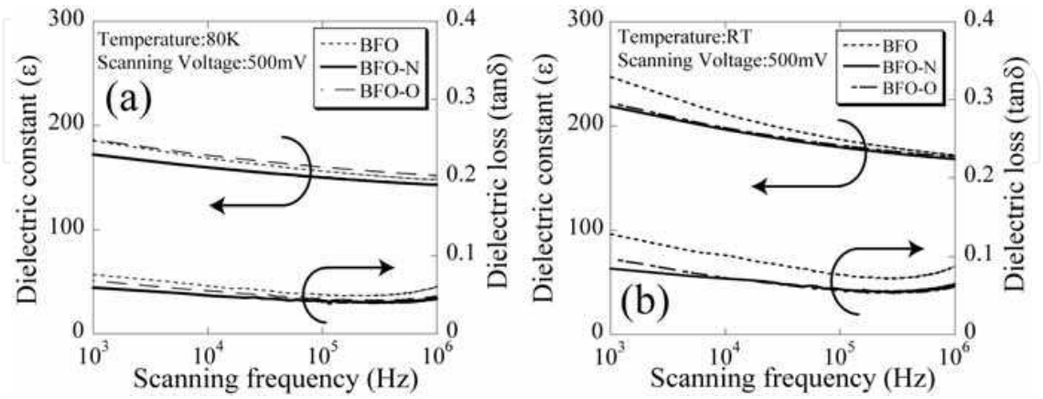

Fig. 14. Dielectric constant-frequency (ε-F) characteristics of $BiFeO_3$ thin films measured at (a) 80 K and at (b) RT.

Figures 15(a) and 15(b) show P-E hysteresis loops of $BiFeO_3$ thin films measured at (a) 80 K and at (b) RT with a scanning frequency of 20 kHz. The remanent polarizations (P_r) measured at 80 K under the maximum applied electric field of 1.2 MV/cm are 91, 87, and 89 μC/cm² for the films of BFO, BFO-N, and BFO-O, respectively. In addition, the double coercive field ($2E_c$) is reduced at about 90 kV/cm in the nitrogen-annealed film. The slight reduction of coercive field is also observed at RT, as shown in Fig. 15(b). This reduction of the coercive field may be due to the improvement of the contact between the Pt electrode and the $BiFeO_3$ film or the reduction in defects near the interface between $BiFeO_3$ film and the Pt electrode, as mentioned above.

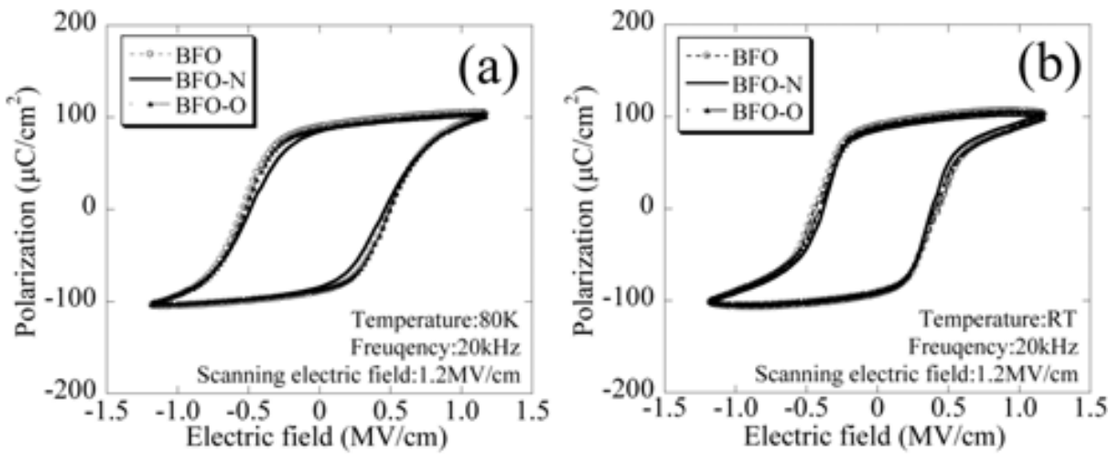

Fig. 15. P-E hysteresis loops measured at (a) 80 K and at (b) RT under 20 kHz triangular scanning voltage of as-prepared (BFO), N_2 annealed (BFO-N), and O_2 annealed (BFO-O) $BiFeO_3$ thin films.

4.3 Improvement of ferroelectric property of $BiFeO_3$ thin films by electric filed application

To evaluate the effect of the electric field application, *P-E* hysteresis loops were measured at 80 K in a following order; the first measurement was carried out by the applied voltage from 5 to 70 V, which corresponds to 0.2 MV/cm to 2.8 MV/cm, and then, the second measurement was carried out from 70 to 5 V with 1 kHz triangular wave. The temperature was set at 80 K to reduce the thermal effect and to apply high electric field. This measurement was carried out for the BFO-N film because it has the best insulation and ferroelectric characteristics among three films. Figures 16(a-d) show hysteresis changes in BFO-N film before (black lines) and after (red lines) applying the electric field of 0.4, 1.2, 2.0, and 2.8 MV/cm corresponding 10, 30, 50, and 70 V, respectively at 80 K. After applying the electric field of 2.8 MV/cm, which corresponds to 70 V, the shape of hysteresis loop is dramatically changed in the second measurement. In the sequence from Figs. 16(a-d), the remanent polarizations of the first measurement are 0.19, 29.9, 74.5, and 104 μC/cm² under the maximum field of 0.4, 1.2, 2.0, and 2.8 MV/cm, respectively. In addition, the remanent polarizations of the second measurement are 17.4, 84.4, 97.6, and 106.5 μC/cm² under the maximum field of 0.4, 1.2, 2.0, and 2.8 MV/cm, respectively.

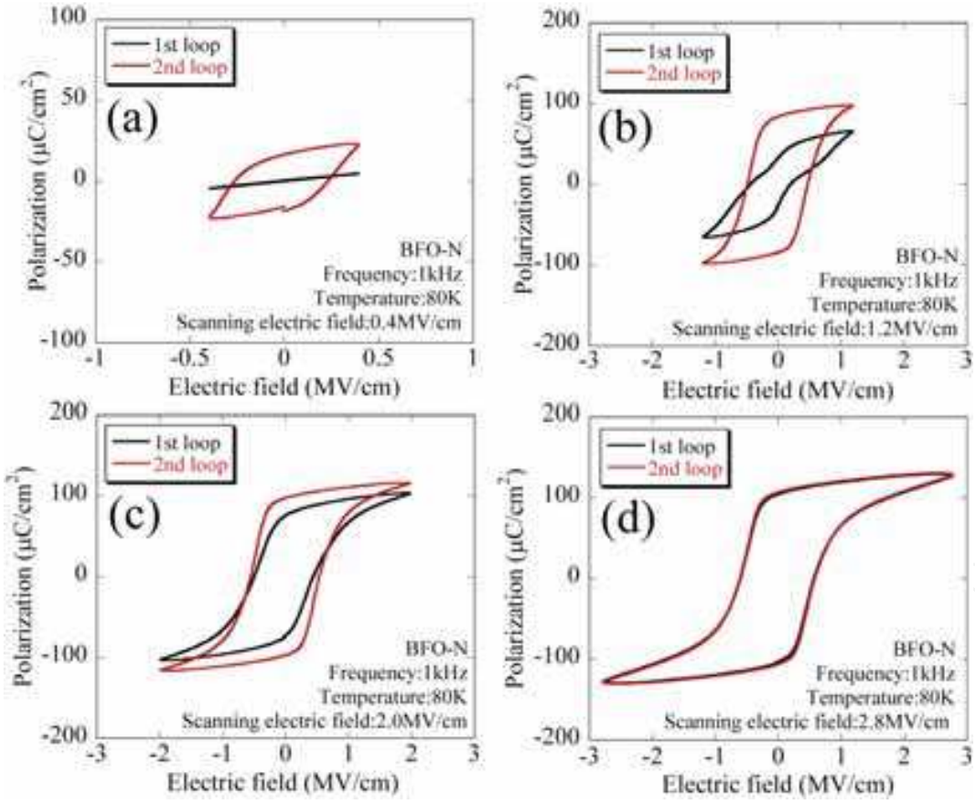

Fig. 16. *P-E* hysteresis of $BiFeO_3$ thin films measured at 80 K under the maximum field of (a) 0.4 MV/cm (10 V), (b) 1.2 MV/cm (30 V), (c) 2.0 MV/cm (50 V), and (d) 2.8 MV/cm (70 V), respectively. Hysteresis loops were measured from 5 to 70 V the first measurement and then measured from 70 to 5 V the second measurement.

Moreover, the leakage current is reduced at about 1 order of magnitude after the *P-E* measurement, as shown in Fig. 17. Dependences of P_r and E_c on the applied electric field are

shown in Fig. 18. P_r and E_c obtained in the first measurement are gradually increased with increase in the electric field, and then, the second measurement keeps large P_r value even in lower electric field. The third measurement from 5 to 70 V was carried out and values of P_r and E_c are almost the same as the second data, as shown in Fig. 18. Kohli et al. reported that the hysteresis of the PZT thin film was changed by applying pulse electric field because of the removal of 90° domain pinning (Kohli et al., 1998). Okamura et al. reported that the wake-up phenomenon, which shows an increase in the remanent polarization by applying switching pulses and removing the locked polarizations in the $SrBi_2Ta_2O_9$ film (Okamura et al., 2000). The improvement of ferroelectricity is possibly due to the relaxation of pinned domains or locked polarizations in the $BiFeO_3$ film by applying high electric field.

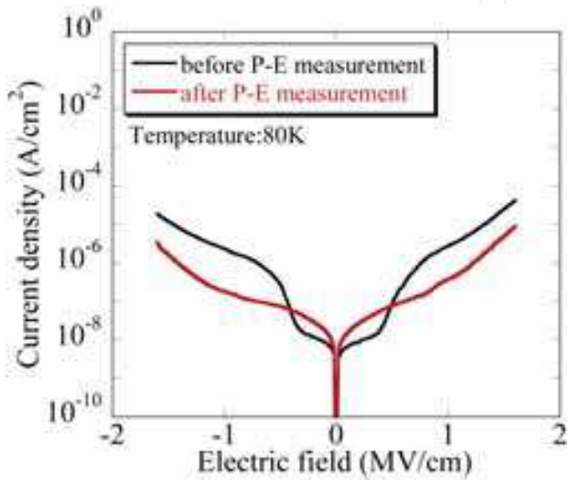

Fig. 17. Current density-electric field (*J-E*) characteristics of $BiFeO_3$ thin films measured at 80 K. The measurement was carried out before and after the *P-E* measurement shown in Fig. 5 (d).

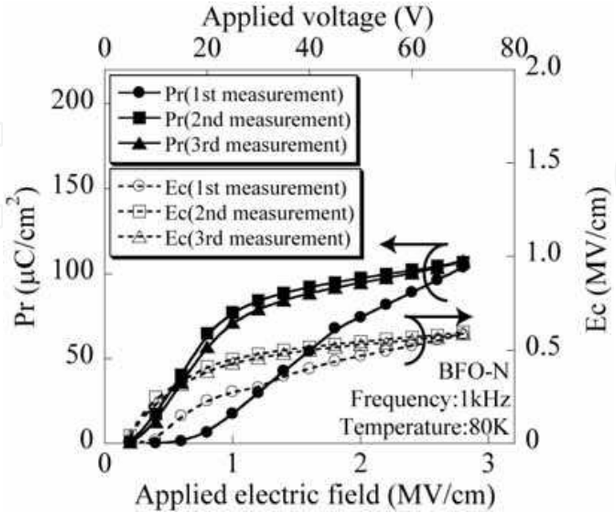

Fig. 18. Applied field dependences of remanent polarization and coercive field at 80 K for the first, the second, and the third measurement.

5. Conclusion

We describe $BiFeO_3$ thin films prepared by CSD with several approaches to improve its ferroelectricity. Controlling Bi/Fe ratio in the precursor solution contributes the promotion of the film crystallization and shows a large polarization of 85 μC/cm² with 10 mol% Bi-excess solution. Insertion of the 10 mol% Bi-excess layer to the stoichiometric $BiFeO_3$ films also promotes the film crystallization, leading to the improvement of the ferroelectricity. Ferroelectric property of films using 10 mol% Bi-excess solution can further improve by the postmetallization annealing as well as the electric field application. These are the effective methods to improve ferroelectricity of $BiFeO_3$.

6. Acknowledgments

The authors thank Takaaki Nakamura, Hideo Fukumura, and Professor Hiroshi Harima of Kyoto Institute of Technology for conducting Raman spectroscopy.

7. References

Roginskaya, Yu. E.; Venevtsev, Yu. N.; Fedulov, S.A. & Zhdanov, G.S. (1963). *Soviet Physics Crystallography,* 8, 610

Palai, R.; Katiyar, R. S.; Schmid, H.; Tissot, P.; Clark, S. J.; Robertson, J.; Redfern, S. A. T., Catalan, G. & Scott, J. F. (2008). β phase and γ–β metal-insulator transition in multiferroic $BiFeO_3$. *Physical Review B,* 77, 014110-1-014110-11

Teague, J. R.; Gerson, R. & James, W. J. (1970). DIELECTRIC HYSTERESIS IN SINGLE CRYSTAL $BiFeO_3$. *Solid State Communications*, 8, 1073-1074

Lebeugle, D.; Colson, D.; Forget, A. & Viret, M. (2007). Very large spontaneous electric polarization in $BiFeO_3$ single crystals at room temperature and its evolution under cycling fields. *Applied Physics Letters*, 91, 022907-1-022907-3

Shvartsman, V. V.; Kleemann, W.; Haumont, R. & Kreisel, J. (2007). Large bulk polarization and regular domain structure in ceramic $BiFeO_3$. *Applied Physics Letters*, 90, 172115-1- 172115-3

Wang, J.; Neaton, J. B.; Zheng, H.; Nagarajan, V.; Ogale, S. B.; Liu, B.; Viehland, D.; Vaithyanathan, V.; Schlom, D. G.; Waghmare, U. V.; Spaldin, N. A.; Rabe, K. M.; Wuttig, M. & Ramesh, R. (2003). Epitaxial $BiFeO_3$ Multiferroic Thin Film Heterostructures. *Science*, 299, 1719-1722

Li, J.; Wang, J.; Wuttig, M.; Ramesh, R.; Wang, N.; Ruette, B.; Pyatakov, A. P.; Zvezdin, A. K. & Viehland, D. (2004). Dramatically enhanced polarization in (001), (101), and (111) $BiFeO_3$ thinfilms due to epitiaxial-induced transitions. *Applied Physics Letters*, 84, 5261-5263

Yun, K. Y.; Ricinschi, D.; Kanashima, T.; Noda, M. & Okuyama, M. (2004). Giant Ferroelectric Polarization Beyond 150 μC/cm² in $BiFeO_3$ Thin Film. *Japanese Journal of Applied Physics,* 43, L647-L648

Ederer, C. & Spaldin, N. A. (2005). Effect of Epitaxial Strain on the Spontaneous Polarization of Thin Film Ferroelectrics. *Physical Review Letters*, 95, 257601-1-257601-4

Ricinschi, D.; Yun, K. Y. & Okuyama, M. (2006). A mechanism for the 150 μC/cm² polarization of BiFeO3 films based on first-principles calculations and new structural data. *Journal of Physics: Condensed Matter*, 18, L97-L105

Schwartz, W. R. (1997). Chemical Solution Deposition of Perovskite Thin Films. *Chemistry of Materials*, 9, 2325-2340

Nakamura, Y.; Yun, K. Y.; Nakashima, S. & Okuyama, M. (2007). Sol-Gel Preparation and Characterization of Multiferroic $BiFeO_3$ Thin Films with Various Bi/Fe Ratio. *Integrated Ferroelectrics*, 95, 226-233

Nakamura, Y.; Nakashima, S. & Okuyama, M. (2008). Influences of Surface Texture and Bi/Fe Ratio on Electric Properties of $BiFeO_3$ Thin Films Prepared by Chemical Solution Deposition. *Japanese Journal of Applied Physics,* 47, 7250-7253

Nakamura, Y.; Nakashima, S.; Ricinschi, D. & Okuyama, M. (2007). The Effect of Bi-excess Surface Layers on $BiFeO_3$ Thin Films Prepared by Chemical Solution Deposition. *2007 MRS Fall Proceedings*, 1034-K11-10

Nakamura, Y.; Nakashima, S.; Ricinschi, D. & Okuyama, M. (2008). THE INSERTION EFFECT OF Bi-EXCESS LAYERS ON STOICHIOMETRIC $BiFeO_3$ THIN FILMS PREPARED BY CHEMICAL SOLUTION DEPOSITION. *Functional Materials Letters*, 1, 19–24

Nakamura, Y.; Nakashima, S. & Okuyama, M. (2009). Improvement of ferroelectric properties of $BiFeO_3$ thin films by postmetallization annealing and electric field application. *Journal of Applied Physics*, 105, 061616-1-061616-4

Alkoy, E. M.; Alkoy, S. & Shiosaki, T. (2005). Effects of Ce, Cr and Er Doping and Annealing Conditions on the Microstructural Features and Electrical Properties of $PbZrO_3$ Thin Films Prepared by Sol–Gel Process. *Japanese Journal of Applied Physics*, 44, 6654-6660

Grossmann, M; Lohse, O; Bolten, D; Boettger, U.; Schneller, T. & Waser, R. (2002). The interface screening model as origin of imprint in $PbZr_xTi_{1-x}O_3$ thin films. I. Dopant, illumination, and bias dependence. *Journal of Applied Physics*, 92, 2680-2687

Abe, K. & Komatsu, S. (1993). Dielectric Constant and Leakage Current of Epitaxially Grown and Polycrystalline $SrTiO_3$ Thin Films. *Japanese Journal of Applied Physics,* 32, 4186-4189

Lee, E. J. H.; Pontes, F. M.; Leite, E. R.; Longo, E.; Magnani, R.; Pizani, P. S. & J. A. Varela (2004). Effects of post-annealing on the dielectric properties of Au/BaTiO3/Pt thin film capacitors. *Materials Letters*, 58, 1715–1721

Joo, J. H.; Jeon, Y. C.; Seon, J. M.; Oh, K. Y.; Roh, J. S. & Kim, J. J. (1997). Effects of Post-Annealing on the Conduction Properties of Pt/(Ba, Sr)TiO_3/Pt Capacitors for Dynamic Random Access Memory Applications. *Japanese Journal of Applied Physics*, 36, 4382-4385

Chung, H. J. ; Chung, S. J.; Kim, J. H. & Woo, S. I. (2001). The effect of post-annealing on the electrical properties of (Pb,Sr)TiO_3 thin films prepared by liquid source misted chemical deposition for ultra large-scale integration (ULSI) Dynamic random access memory (DRAM) capacitor. *Thin Solid Films*, 394, 213-218.

Thakoor, S. (1994). Enhanced fatigue and retention in ferroelectric thin film memory capacitors by post–top–electrode anneal treatment. *Journal of Applied Physics*, 75, 5409-5414

Kamel, T. M.; Kools, F. X. N. M. & With, G. (2007). *Journal of the European Ceramic Society*, 27, 2471–2479

Kohli, M.; Muralt, P. & Setter, N. (1998). Removal of 90° domain pinning in (100) $Pb(Zr_{0.15}Ti_{0.85})O_3$ thin films by pulsed operation. *Applied Physics Letters*, 72, 3217-3219

Okamura, S.; Takaoka, M.; Nishida, T. & Shiosaki, T. (2000). Increase in Switching Charge of Ferroelectric $SrBi_2Ta_2O_9$ Thin Films with Polarization Reversal. *Japanese Journal of Applied Physics*, 39, 5481-5484

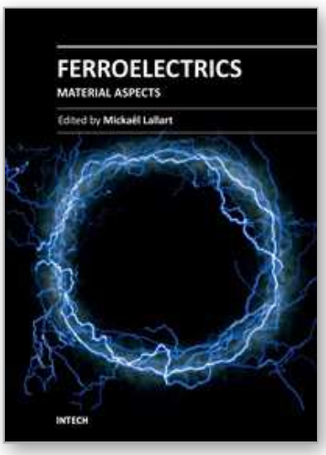

Ferroelectrics - Material Aspects

Edited by Dr. MickaÃ«l Lallart

ISBN 978-953-307-332-3
Hard cover, 518 pages
Publisher InTech
Published online 24, August, 2011
Published in print edition August, 2011

Ferroelectric materials have been and still are widely used in many applications, that have moved from sonar towards breakthrough technologies such as memories or optical devices. This book is a part of a four volume collection (covering material aspects, physical effects, characterization and modeling, and applications) and focuses on ways to obtain high-quality materials exhibiting large ferroelectric activity. The book covers the aspect of material synthesis and growth, doping and composites, lead-free devices, and thin film synthesis. The aim of this book is to provide an up-to-date review of recent scientific findings and recent advances in the field of ferroelectric materials, allowing a deep understanding of the material aspects of ferroelectricity.

InTech Europe
University Campus STeP Ri
Slavka Krautzeka 83/A
51000 Rijeka, Croatia
Phone: +385 (51) 770 447
Fax: +385 (51) 686 166
www.intechopen.com

InTech China
Unit 405, Office Block, Hotel Equatorial Shanghai
No.65, Yan An Road (West), Shanghai, 200040, China
中国上海市延安西路65号上海国际贵都大饭店办公楼405单元
Phone: +86-21-62489820
Fax: +86-21-62489821

IntechOpen